



City Research Online

City, University of London Institutional Repository

Citation: Theodorakakos, A., Strotos, G., Mitroglou, N., Atkin, C. & Gavaises, M. (2014). Friction-induced heating in nozzle hole micro-channels under extreme fuel pressurisation. *Fuel*, 123, pp. 143-150. doi: 10.1016/j.fuel.2014.01.050

This is the accepted version of the paper.

This version of the publication may differ from the final published version.

Permanent repository link: <https://openaccess.city.ac.uk/id/eprint/13585/>

Link to published version: <https://doi.org/10.1016/j.fuel.2014.01.050>

Copyright: City Research Online aims to make research outputs of City, University of London available to a wider audience. Copyright and Moral Rights remain with the author(s) and/or copyright holders. URLs from City Research Online may be freely distributed and linked to.

Reuse: Copies of full items can be used for personal research or study, educational, or not-for-profit purposes without prior permission or charge. Provided that the authors, title and full bibliographic details are credited, a hyperlink and/or URL is given for the original metadata page and the content is not changed in any way.

City Research Online:

<http://openaccess.city.ac.uk/>

publications@city.ac.uk

Friction-induced heating in nozzle hole micro-channels under extreme fuel pressurisation

Andreas Theodorakakos, George Strotos, Nicholas Mitroglou, Chris Atkin, Manolis Gavaises*

School of Engineering and Mathematical Sciences, City University London, Northampton Square, London EC1V 0HB, UK

A B S T R A C T

Fuel pressurisation up to 3000 bar, as required by modern Diesel engines, can result in significant variation of the fuel physical properties relative to those at atmospheric pressure and room temperature conditions. The huge acceleration of the fuel as it is pushed through the nozzle hole orifices is known to induce cavitation, which is typically considered as an iso-thermal process. However, discharge of this pressurised liquid fuel through the micro-channel holes can result in severe wall velocity gradients which induce friction and thus heating of the liquid. Simulations assuming variable properties reveal two opposing processes strongly affecting the fuel injection quantity and its temperature. The first one is related to the de-pressurisation of the fuel; the strong pressure and density gradients at the central part of the injection hole induce fuel temperatures even lower than that of the inlet fuel temperature. On the other hand, the strong heating produced by wall friction increases significantly the fuel temperature; local values can exceed the liquid's boiling point and even induce reverse heat transfer from the liquid to the nozzle's metal body. Local values of the thermal conductivity and heat capacity affect the transfer of heat produced at the nozzle surface to the flowing liquid. That creates strong temperature gradients within the flowing liquid which cannot be ignored for accurate predictions of the flow through such nozzles.

Keywords: High fuel pressurisation, Variable fuel properties, Flow-induced boiling, Cavitation, Fuel injection

1. Introduction

The development of direct injection (DI) Diesel engines over the last 20 years has been remarkable. The market share of Diesels has been increasing for passenger cars while it dominates in the medium and heavy duty vehicles. According to an Energy Outlook Review for 2040 [1], the number of such vehicles is expected to significantly increase (more than double) over the next decades; this increase is linked with the expected growth of the construction sector in the developing countries, the continued development of highly-populated urban areas that require increased transportation

of goods by road/rail and the increase in the transportation of goods by sea. It is also expected that the consumption of Diesel fuel from this particular sector will double. As a result, there is great concern about the durability of the fuel injection equipment for medium and heavy duty applications [2], which can be impaired by the appearance of aggressive cavitation within the Diesel injector nozzles. At the same time, increasingly stringent emission legislations such as Euro VI, EPA10, J-PNLT and Stage IV/Tier 4 and the forthcoming regulations on CO₂ are contributing to the development of more efficient IC engines. Advancements towards 2500/3000 bar injection pressure have become a reality [3,4] as this results to simultaneous reduction of soot and NO_x emissions and thus, put less demand on the efficiency and cost of after-treatment systems.

* Corresponding author. Tel.: +44 2070408115.

E-mail address: m.gavaises@city.ac.uk (M. Gavaises).

Nomenclature

Symbols

α_L	ratio of liquid volume to cell volume
U	internal energy (J/kg)
c_d	nozzle discharge coefficient
c_p	heat capacity under constant pressure (J/(kg K))
c_{pmT}	mean heat capacity under constant pressure between temperature T and reference temperature T_0 (J/(kg K))
Q_{vis}	viscous work (W/m ³)
h	enthalpy (J/kg)
k	thermal conductivity (W/(mK))
κ	turbulent kinetic energy (m ² /s ²)
p	pressure (Pa)
\vec{q}	thermal diffusion vector (W/m ²)
T	temperature (K)
t	time (s)

\vec{u}	velocity vector (m/s)
μ	molecular viscosity (kg/(m s))
ρ	density (kg/m ³)
σ	Prandtl number
$\vec{\tau}_{eff}$	stress tensor (Pa)
\mathcal{I}	unit tensor

Subscripts

0	property at reference pressure p_0 and temperature T_0
eff	effective property
t	turbulent property

Superscripts

'	fluctuation
---	-------------

The occurrence of cavitation in Diesel fuel injectors has been documented in the open literature since the late 1990s, for example [5]. Cavitation is known to affect nozzle efficiency, fuel atomisation and spray development. Numerous past studies have examined both experimentally and computationally this phenomenon; however, only limited information is available in the open literature about cavitation effects on system durability and erosion at elevated injection pressures. The cavitating flow in fuel injection systems is typically characterised by a large number (of the order of 10^5 – 10^6 during a typical injection event) of bubbles exposed to pressure differences reaching 3000 bar. As a result of the violent change in the cavitation bubble size during their collapse, pressures and temperatures may even exceed 1 GPa and 10^4 – 10^5 K, respectively [6]. Cavitation bubble collapse often produces shock waves strong enough to cause surface erosion. As a result, today's injectors incorporate tapered holes that converge towards the hole exit and which are known to suppress cavitation. Due to the difficulty in obtaining real-time measurements during the injection process, most of the experimental studies reported (selectively [7–11]) refer to experimental devices emulating operating conditions similar to those of Diesel engines. Limited information exists for production injectors during engine operation although recent advances in testing equipment (for example, high speed cameras with 10^6 fps) and use of X-rays [12] are expected to improve our understanding in the near future. Therefore, development and use of computational fluid dynamics models predicting the flow in such systems seem to be the only route for obtaining information about the details of the nozzle flow under realistic operating conditions. Modelling efforts aiming to tackle cavitation under such hostile environments have been a challenge for many years. Within the approach of [13] the cavitating fluid was treated as mixture, assuming the existence of small bubble clouds on a sub-grid scale. In the model of [14], instead of treating cavitating fluid as a single mixture, the two-fluid method is employed; two sets of conservation equations are solved, one for the liquid and one for the vapour phase. With this approach the two phases can have different velocities. In [15] another bubble-based cavitation model has been proposed and implemented in commercial CFD codes. Another variant of the bubble model is the approach of [16,17]. In this case the authors modified the classical interface-capturing Volume of Fluid (VOF) method by considering the transported scalar volume fraction to be the local vapour fraction of a bubble cloud. More recent important advances (selectively [18–21]) have proposed models that account for collective compressibility and shock wave interaction effects in poly-dispersed cavitating flows. Recently, more fundamental models have been developed to simulate the

shock waves produced during the non-spherical bubble collapse processes [22] but they cannot be directly linked to flows comprising millions of cavitation bubbles. Eulerian–Lagrangian cavitation models are also available. They are based on the implementation of various versions of the Rayleigh–Plesset bubble dynamics equation (selectively [23–25]) for predicting the bubble growth and collapse which is important if heating effects and the implications on erosion are to be considered.

All previous cavitation models assumed iso-thermal flow conditions, which was justified on the basis that cavitation takes place over very short time scales and the fact that the residence time of the liquid within the injection holes is so short that heat transfer with the surrounding could be neglected. However, as the trend in technology is towards pressures in the excess of 2500 bar and possibly reaching 3000 bar, the common assumption of isothermal flow conditions within the context of phase-change through cavitation may no longer be valid. It is now believed that due to this high fuel pressure, the extreme velocities occurring during the discharge of the liquid through the nozzle's micro-channel holes can induce wall friction which leads in turn to significant fuel heating. In some cases this may lead to boiling of the flowing fluid. Boiling heat transfer has been an active research topic in the last decade. However, only limited number of papers deal with pool boiling at high pressures, such as [26] involving experimental campaigns at pressure up to 70 bar. The highest pressure in flow boiling was achieved by [27]; this work proposed a correlation for the evaluation of the heat transfer coefficient for boiling at pressures up to 90 bar. It seems that no data are available for higher pressure systems, such as those used in fuel injection systems, and therefore there is currently no relevant model available for simulating boiling under such pressure conditions.

The present study challenges these assumptions and shows that under such extreme fuel pressurisation and subsequent discharge through the nozzle's micro-channel holes, production of heat caused by wall friction can induce temperatures above the boiling point of the flowing fuel, and thus, significantly alter the flow regimes believed to prevail in such systems. Thus, the main focus of this work is to assess such effects. The group at City University London has developed previously its own CFD/cavitation model based on a coupled Eulerian–Lagrangian stochastic approach [28]; this model provides the platform for the present work. It is also linked with the early computational advances reported in [29] predicting the influence of fuel properties on cavitation when extreme fuel pressurisation up to 2500 bar was utilised. The next section gives the description of the computational model developed to account for variable fuel properties and heating effects;

this is followed by a description of the results obtained, which provide a detailed understanding of the processes involved and reveal the possible occurrence of new flow regimes within such systems. The sound conclusions are summarised at the end.

2. Computational model

The flow solver utilised has been developed by the authors and simulated the 3-D flow using the finite volume approximation. The liquid flow is described by the Navier–Stokes and energy conservation equations considering the influence of ratio of liquid volume to cell volume α_L ; the numerical methodology has been reported in [28] and it is not repeated here; these equations are not repeated here and focus is given only to the inclusion of the energy equation employed for estimating the temperature changes during the injection process. As the flow is turbulent, the standard κ – ϵ model of turbulence has been utilised with standard wall functions. Turning now to the non-isothermal case, the energy conservation equation was utilised. Based on [30], the conservation equation for enthalpy is:

$$\frac{\partial}{\partial t}(\alpha_L \rho h) + \nabla \cdot (\alpha_L \rho h \vec{u}) = -\nabla \cdot \vec{q}_{eff} + Q_{vis} + \frac{D(\alpha_L p)}{Dt} + S_h \quad (1)$$

This equation is also consistent with the enthalpy equation given in [31] for the case of single-phase flow and S_h is a source term which contains terms related to the presence of the secondary phase [30]. The diffusion term including the effects of turbulence is expressed as:

$$\nabla \cdot \vec{q}_{eff} = \nabla \cdot (-\alpha_L k_{eff} \nabla T) \quad (2)$$

where k_{eff} the effective thermal conductivity, calculated as $k_{eff} = k + c_p \frac{\mu_t}{\sigma_t}$ with $\sigma_t = 0.85$.

In addition, Q_{vis} is the work done by irreversible viscous forces (commonly known as viscous heating):

$$Q_{vis} = \bar{\tau}_{eff} : \nabla \vec{u} = \sum_i \sum_j \bar{\tau}_{eff,ji} \frac{\partial u_j}{\partial x_i} \quad (3a)$$

$$\bar{\tau}_{eff} = \alpha_L \mu_{eff} (\nabla \vec{u} + (\nabla \vec{u})^T) - \frac{2}{3} (\alpha_L \rho \kappa + \alpha_L \mu_{eff} \nabla \vec{u}) \mathcal{I} \quad (3b)$$

The general formulation for enthalpy is:

$$dh = \left(\frac{\partial h}{\partial T} \right)_p dT + \left(\frac{\partial h}{\partial p} \right)_T dp = c_p dT + \left(\frac{\partial h}{\partial p} \right)_T dp \quad (4)$$

The above can be integrated taking into account that the final result does not depend on the integration path [32]. Assuming that h_0 is the enthalpy at reference pressure and temperature p_0 and T_0 we get:

$$h - h_0 = \int_{T_0}^T c_p dT + \int_{p_0}^p \left(\frac{\partial h}{\partial p} \right)_T dp \quad (5)$$

The second integral over p is for constant temperature T_0 whilst the first integral over T is for constant pressure p . The integral over T can be calculated using the mean specific heat c_p between temperatures T_0 and T :

$$\int_{T_0}^T c_p dT = c_{pmT} (T - T_0) \quad (6)$$

where

$$c_{pmT} = \frac{\int_{T_0}^T c_p dT}{T - T_0} \quad (7)$$

Finally, the enthalpy can be rewritten as:

$$h - h_0 = c_{pmT} (T - T_0) + h^* \quad (8)$$

where

$$h^* = \int_{p_0}^p \left(\frac{\partial h}{\partial p} \right)_T dp \quad (9)$$

The term h^* is a function of pressure. For the case of an ideal gas it is identically zero, while for the case of a constant density fluid it is $h^* = (p - p_0)/\rho$. Finally, an equation for temperature can be obtained by using Eq. (1) along with the expression for enthalpy (Eq. (8)):

$$\begin{aligned} \frac{\partial}{\partial t} (\alpha_L \rho c_{pmT} (T - T_0)) + \nabla \cdot (\alpha_L \rho c_{pmT} (T - T_0) \vec{u}) = \\ - \nabla \cdot (\vec{q}_{eff}) + \frac{D(\alpha_L p)}{Dt} - \left(\frac{\partial}{\partial t} (\alpha_L \rho h^*) + \nabla \cdot (\alpha_L \rho h^* \vec{u}) \right) + Q_{vis} + S_h \end{aligned} \quad (10)$$

In Eq. (10) above, a term containing the h^* appears, which is a function of pressure and vanishes for the case of an ideal gas, while for the case of incompressible fluid it cancels out with the pressure term. The above equation is solved iteratively, where the values of ρ , μ , k , c_{pmT} and h^* are updated using the available polynomial fits with the latest calculated values of p and T , after each iteration [32]. Those polynomial fits correspond to property measurements for summer Diesel fuel; they are experimentally verified for pressures between 0 and 2400 bar and temperatures between 20 and 120 °C. Extrapolation is also possible for temperature/pressure values outside this range as apparently needed for addressing pressures up to 3000 bar and temperatures up to 240 °C. As mentioned, rising pressure causes considerable variations to all properties. Density changes up to 15% while viscosity increases by an order of magnitude for the lower temperature case but differences become smaller with increasing initial fuel temperature. Heat capacity is not affected significantly by fuel pressure but increases by a substantial 20% when temperature increases approximately 100 °C. On the contrary, the increase of thermal conductivity with pressure indicates that heat conduction within the flowing liquid will be enhanced as pressure increases. A includes the relations used and the trends are plotted in [33].

With regards to the implementation of variable flow properties in the flow solver, the following procedure has been followed. The implementation of variable viscosity was straightforward, due to the usage of RANS turbulence modelling. Therefore, at each fluid location the local laminar viscosity is updated according to the local pressure and temperature. Regarding compressibility, the necessary changes to the continuous phase solver mainly affect the discretisation of the continuity equation which has to be altered. As mentioned in [28], the continuity and momentum equations are coupled through the pressure correction method and are solved sequentially following an iterative segregated algorithm. In order to account for compressibility, the classical pressure correction method had to be extended following the work of [34–36]. Within the context of the classical approach one needs to discretise the convective term of the continuity equation and link velocity with pressure. Typically, one writes velocity as follows:

$$u = u^* + u' \quad (11)$$

where u^* is the previous known velocity value and u' is the required velocity correction which needs to be linked with pressure. For the aforementioned compressible extension of the pressure correction method one needs to introduce an additional correction for the density, in the discretisation of the convective term. Following [34–36] we have:

$$\rho u = (\rho^* + \rho') (u^* + u') = \rho^* u^* + \rho^* u' + \rho' u^* + \rho' u' \quad (12)$$

or alternatively

$$(\rho^* + \rho')(u^* + u') = \rho u^* + \rho^* u - \rho^* u^* + \rho' u' \quad (13)$$

It is crucial for the derivation of the compressible extension to the pressure correction scheme to have a linear coupling between density and pressure; the presence of this coupling depends solely on the equation of state of the considered fluid. Given that through discretisation of the continuity equation one seeks to eventually arrive at a linear pressure equation, both velocity and density, whose values are still unknown, need to be expressed as linear functions of pressure. The employed non-linear equations have been linearised by neglecting higher order terms as these approach zero when the solution has converged. For the discretisation of the convective term, interpolation is needed; in the current study the 'upwind' scheme has been used for the interpolation of pressure in the discretised form of the continuity equation. Finally, as cavitating flows are inherently transient in nature, time-dependent simulations have been performed in order to account for the two-phase flow development within the nozzle even at fixed geometry and pressure boundary conditions, as explained in [28]. The weak temporal gradients for such pseudo-steady-state conditions justify the use of a simple 1st order implicit Euler discretisation scheme for modelling the time derivatives of the solved equations. Regarding spatial discretisation, the 2nd order scheme of [37] has been used.

For the estimation of the cavitation vapour volume fraction, again the approach followed in [28] is adopted, so it is not repeated here. Emphasis here is given only to effects associated with the variation of fluid's physical properties due to excess pressurisation and heating produced during the discharge of the fuel through the nozzle's micro-channels.

3. Simulation cases

A typical nozzle which incorporates 6 micro-channel holes with diameter of 0.175 mm has been used for the purposes of the present investigation; a similar version of this nozzle has been utilised in the past in order to obtain visualisation data for the cavitation development and LDV measurements of the liquid velocity; these data obtained at much lower pressures have been utilised in the past for validation of the iso-thermal cavitation model [38] and they are not repeated here. The nozzle features inlet rounding, tapered holes and has a relatively high discharge coefficient c_d of around 0.88. The numerical grid employed is shown in Fig. 1; it

consists of approximately one million cells; a parametric study has proved that grid-independent results have been obtained for this particular design. Only one of the six hole channels has been simulated; symmetry conditions have been assumed on the corresponding cross sections. Additionally, a fixed needle lift position has been used, which correspond to that of a typical nominal full lift of a production Diesel fuel injector (0.3 mm). The test cases simulated are listed in Tables 1 and 2. The purpose here is initially to compare the results between the solutions obtained using fixed properties under isothermal conditions (incompressible fluid), which is the common assumption adopted in such simulation reported in the literature, with those obtained using variable properties being function of local pressure and temperature. Moreover, the effect of viscous heating has been considered by employing adiabatic walls as the nozzle's wall temperature is practically unknown, although manufacturing and operating constraints limit it to temperatures below 230 °C; these correspond to the cases listed in Table 1. In addition, the effect of initial fuel temperature

Table 1

Test cases for quantifying the effect of fuel variable fuel properties and wall heat transfer; constant injection pressure of 2400 bar and fixed inlet temperature of 80 °C

Case	Temperature		Properties ρ, μ, c_p, k
	Fixed or variable	Viscous heating	
1	Fixed	No	Fixed
2	Variable	No	Variable
3	Variable	Yes	Variable

Table 2

Test cases for quantifying the effect of injection pressure and inlet temperature; adiabatic walls and variable fuel properties have been assumed.

Case	Inlet pressure	Inlet temperature (°C)
4	2400	25
5	3000	25
6	1600	80
7	2000	80
3	2400	80
8	3000	80
9	2400	120
10	3000	120

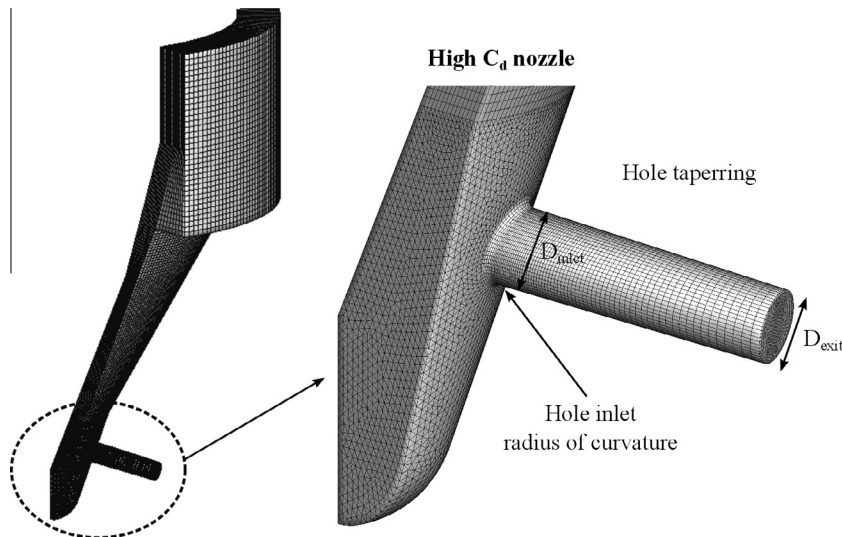


Fig. 1. Numerical grid of the 60° sector of Diesel nozzle simulated; the high c_d nozzle features a curved hole inlet and hole tapering. Reproduced from [33].

as a result of fuel pressurisation has been examined. As in practice the fuel temperature entering the nozzle is controlled by the design of the fuel system including its cooling circuit, it can only be given here as an initial condition to the present simulation model. Typical values considered are of the order of 80 °C, but here values from 25 °C to 120 °C have been explored. The influence of those parameters as function of injection pressure, ranging between 1600 and 3000 bar, and fuel temperature at the rail has been also considered; these test cases are summarised in Table 2. For all simulations performed, a fixed pressure of 60 bar has been adopted at the downstream boundary of the hole exit, as this can be considered a typical value during the injection period in Diesel engines.

4. Results and discussion

In this section, the results obtained with the model are presented in two sections. In the first section, comparison of the CFD against 0-D estimates of the fuel heating through nozzles is performed in order to gain confidence in the model in the absence of experimental data. In the following section, particular 3-D flow structures identified are described in order to gain a better physical understanding of the underlying processes.

4.1. Comparison against 0-D models

For fuel pressurisation up to 3000 bar followed by discharge through injection hole micro-channels of the order of 150 μm , and during transient injection events lasting no more than 1 ms, no experimental data for the local (or even bulk) fuel temperature distribution are currently available. Thus, in order to get some confidence on the predictive capability of the developed model, comparison between the 3-D model predictions against those obtained from a 0-D analysis for the bulk heating of liquid discharging through nozzle micro-channel holes have been obtained. The basic principle of such 0-D simulations is the following: as the flow is accelerated within the injection hole, the liquid pressure is converted into kinetic energy and thermal losses (assuming that turbulent kinetic energy can be neglected). The ratio between the actual injected fuel mass over the ideal one that would have been obtained without any losses define the nozzle discharge coefficient; this relation is shown in Fig. 2. Two lines are plotted, one corresponding to estimates obtained with fixed density and one with variable density as function of pressure and temperature. The shaded areas superimposed on top of this figure indicate the range of expected c_d values for typical Diesel injector nozzles

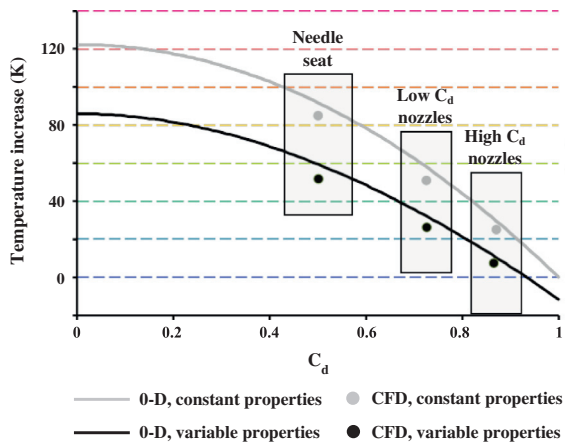


Fig. 2. Diesel temperature increase as function of the discharge coefficient of the flow passage. Reproduced from [33].

currently utilised in various applications. These estimates have been obtained assuming an initial fuel temperature of 80 °C and pressure of 2400 bar, which is the upper limit of the data base of fuel properties available. These estimates predict the strong fuel de-pressurisation that causes fuel acceleration inside the injection hole, and the increase in temperature, particularly for the partial needle opening case of the low c_d nozzle. Liquid compressibility compensates some of the expected fuel heating while, interestingly enough, some cooling is predicted for the compressible case for c_d values close to 1. The difference between the two curves seems to be rather significant, which implies that variable properties are important for accurate estimates of fuel heating. The difference between the 0-D and CFD predictions seem to be small and justifiable, as the CFD models accounts for the turbulent kinetic energy; in addition, the strong gradients of velocity, which will be further discussed in the following section, result in an overall higher liquid kinetic energy compared to that derived assuming a uniform velocity profile.

Having obtained some confidence in the model predictions, we now present in more detail the results obtained for the conditions of Tables 1 and 2. Table 3 summarises the results for the conditions of Table 1. Case 2 includes variable fuel properties but viscous heating is not considered while Case 3 includes both effects. It can be seen that, for both cases, the fuel injection quantity can be significantly overestimated if fixed fuel properties are used. With regards to temperature, when the viscous heating is ignored (case 2) then it is noticeable that the mean fuel temperature decreases, which is a direct result of the de-compression process. When viscous heating is included (case 3) then the mean fuel temperature increases by ~ 15 °C relative to the previous case.

Fig. 3 reveals further the effect of variable fuel properties on liquid temperature, relative to the results obtained when fixed variables are used; this time, for both sets of simulations viscous heating has been included. The plot summarises the minimum

Table 3

Variation of nozzle discharge coefficient, % mass difference and mean exit temperature for the simulations cases of Table 1.

Case	Mass difference	Mean exit temperature difference (°C)
1	Reference case	-
2	-6.5%	-8.0
3	-7.4%	+7.7

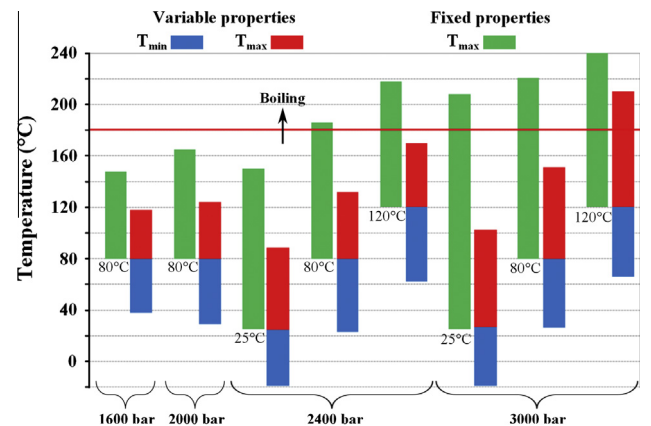


Fig. 3. Variation of minimum and maximum temperatures as calculated by assuming constant fluid properties and variable fluid properties for the simulations cases of Table 2.

and maximum temperature calculated locally within the computational domain for the conditions of Table 2. For the case of the fixed fuel temperatures, significantly higher values of temperature are calculated relative to the case of variable fuel temperature. Since, during the de-pressurisation of the liquid as it enters into the injection holes, there is no mechanism to reduce its temperature, only heating is produced and therefore the temperature never drops below the inlet temperature. On the contrary, when variable properties are utilised, the de-pressurisation of the fuel results in internal cooling while at the same time heat is generated on the wall of the nozzle due to friction. The heat produced increases as fuel pressure increases and in some cases, temperature increases in excess of 180 °C are observed. The boiling point is also indicated on Fig. 3, as taken from [32]; it can be seen that boiling should be expected as pressure increases in excess of 2400 bar, if inlet temperature is not significantly low.

4.2. 3-D flow field

We now proceed to the description of the 3-D flow distribution through such injectors. The following Fig. 4 shows the predicted distribution of four flow variables on the symmetry plane across the injection hole. The variables plotted are (a) the magnitude of the velocity gradient expressed on a logarithmic scale, (b) liquid density, (c) thermal conductivity and (d) liquid viscosity. Some interesting observations can be made. Starting from the spatial velocity gradient, it can be seen that it can attain values of the order of $10^5/s$. These peak values are mainly concentrated on the wall of the nozzle but also in a relatively wide region starting from the upper part of the hole inlet and extending well inside the injection hole. However, at the central part of the injection hole, it can be seen that the velocity gradient is very small, indicating a relatively uniform velocity profile. Liquid density, thermal conductivity and viscosity show all similar trends. As the flow enters the injection hole, density changes from almost 900 kg/m³, which is its value under 3000 bar, down to 720 kg/m³, a change of more

than 15%. A relatively smooth density gradient can be observed, which is a result of the pressure distribution within the injection hole; such tapered nozzle shapes are known to produce a relatively smooth pressure drop, with the only exception being the region just at the upper part of the hole, near the inlet, where pressure drops below the vapour pressure of the fluid and initiates cavitation there. Similarly, the drop in thermal conductivity is more than 50% at the hole exit compared to its corresponding value at 3000 bar, while viscosity drops but almost one order of magnitude. It is thus evident that such strong gradients, function of the local pressure and temperature cannot be ignored if meaningful temperature predictions are to be made. Similarly, the temperature distribution shows strong gradients, as shown in Fig. 5. Some interesting observations can be made here. The central part of the injection hole seems to be at temperatures below the inlet temperature, which is indicated by the highlighted iso-surface. The temperature within this region can be a few degrees below the inlet temperature due to the de-pressurisation of the fuel and the absence of significant velocity gradients that could induce heating. At the same time, the strong wall friction which induced high temperatures around the nozzle wall surface does not penetrate all the way through the nozzle to heat all the fuel. The fact that thermal conductivity takes smaller values at the central part of the injection hole further contributes to less heat flux in this region. Similarly, the high heat capacity values on the nozzle surface (being mainly a strong function of temperature and almost independent from pressure) further contribute to the formation of strong density gradients within the nozzle hole. Thus, a ring of fuel attached to the nozzle wall surface with high temperatures is formed; in this region boiling can be expected to take place depending on the initial fuel temperature and pressure. So far, no study exists to indicate the possible formation of this flow regime in Diesel fuel injectors. Moreover, on these plots, the effect of injection pressure on the induced temperature increase due to wall friction can be also appreciated. It is clear that increasing injection pressure results in higher values of fluid velocity within this confined space and

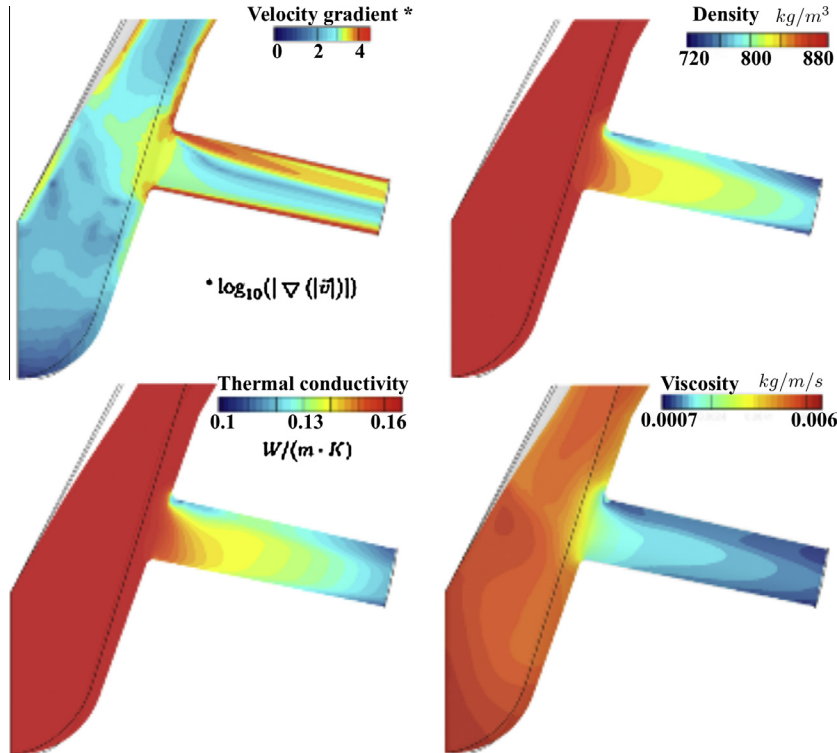


Fig. 4. Distribution of velocity gradient (on a logarithmic scale), density, thermal conductivity and viscosity on the plane of symmetry [$P_{inj} = 3000\text{bar}$, $T_{inj} = 80\text{ }^\circ\text{C}$].

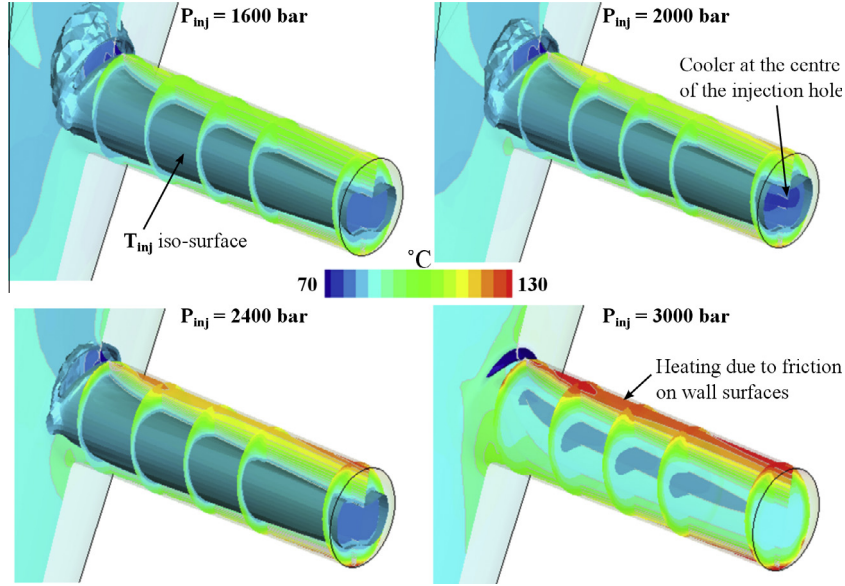


Fig. 5. Distribution of temperature within the nozzle orifice as function of injection pressure; $[T_{inj} = 80 \text{ }^\circ\text{C}]$.

thus formation of sharper gradients and increased friction. The calculated peak temperature increase is of the order of $40 \text{ }^\circ\text{C}/1000 \text{ bar}$ temperature increase.

5. Conclusions

Pressurisation of fuel in modern common-rail injectors reaching 3000 bar results in increased temperatures and significant variation of the physical properties of the fuel (density, viscosity, heat capacity and thermal conductivity) relative to those predicted when fixed fuel properties are used. Such phenomena have been investigated using a CFD model that has challenged the assumption of isothermal conditions in cavitating nozzle flows and has allowed quantification for the first time of such effects. In the absence of experimental data, the model predictions have been compared against 0-D simulations predicting the mean temperature increase as a function of the nozzle discharge coefficient. The CFD predictions have been found to be in good agreement for a range of nozzle discharge coefficients assuming both constant as well as variable fluid properties. Variable properties simulations reveal two opposing processes strongly affecting the fuel injection mass rate and its temperature. The first one is related to the depressurisation of the fuel which may result in internal cooling; the strong pressure and density gradients at the central part of the injection hole indicate zones of fuel with temperature even lower than that of the inlet temperature. On the other hand, the strong heating produced by wall friction increases significantly the fuel temperature; local values can exceed the liquid's boiling point and even induce reverse heat transfer from the liquid to the nozzle's metal body. The heat produced near the nozzle surfaces is transferred to the flowing liquid and it is affected by the thermal conductivity, heat capacity and viscosity values of the fuel which are all strong functions of the local pressure and temperature.

Acknowledgements

The authors would like to acknowledge the contribution of The Lloyd's Register Foundation (The LRF) that supports the activities of the International Institute of Cavitation Research at City University

London; this work has been partly performed at the premises of the Institute.

Appendix A. Correlations for physical properties of fuel

Density:

$$\rho = \sum_{i=1}^3 \sum_{j=1}^3 \alpha_{ij} T^{j-1} p^{i-1} \quad (\text{A.1})$$

$$\mathbf{A} = \begin{pmatrix} 828.59744 & 0.63993 & -0.00216 \\ 8.65679 \times 10^{-7} & -5.93672 \times 10^{-9} & 1.56678 \times 10^{-11} \\ -7.59052 \times 10^{-16} & 8.99915 \times 10^{-18} & -2.77890 \times 10^{-20} \end{pmatrix} \quad (\text{A.2})$$

Specific heat at constant pressure:

$$c_p = \sum_{i=1}^5 \sum_{j=1}^3 d_{ij} T^{j-1} \left(\frac{p}{10^5} \right)^{i-1} \quad (\text{A.3})$$

$$\mathbf{D} = \begin{pmatrix} -977.16186 & 14.025100 & -0.01374 \\ 2.22361 \times 10^{-4} & -1.62143 \times 10^{-4} & 2.23214 \times 10^{-9} \\ -1.96181 \times 10^{-9} & 2.03748 \times 10^{-7} & -1.78571 \times 10^{-14} \\ 4.15000 \times 10^{-14} & -7.54100 \times 10^{-11} & 4.03897 \times 10^{-28} \\ -3.48714 \times 10^{-18} & 1.00688 \times 10^{-14} & -1.47911 \times 10^{-31} \end{pmatrix} \quad (\text{A.4})$$

Enthalpy pressure derivative under constant temperature and pressure integral:

$$\left(\frac{\partial h}{\partial p} \right)_T = \sum_{i=1}^3 \sum_{j=1}^3 c_{ij} T^{j-1} p^{i-1} \quad (\text{A.5})$$

$$\mathbf{C} = \begin{pmatrix} 0.00404 & -1.54245 \times 10^{-5} & 2.20238 \times 10^{-8} \\ -7.34229 \times 10^{-11} & 4.84276 \times 10^{-13} & -8.79805 \times 10^{-16} \\ 2.23591 \times 10^{-19} & -1.60598 \times 10^{-21} & 3.17966 \times 10^{-24} \end{pmatrix} \quad (\text{A.6})$$

$$\int_{p_0}^p \left(\frac{\partial h}{\partial p} \right)_T dp = \sum_{i=1}^3 \frac{1}{i} \sum_{j=1}^3 c_{ij} T^{j-1} (p^i - p_0^i) \quad (\text{A.7})$$

Kinematic viscosity:

$$\log_{10}(10^6 \nu) = 8.67271 - 0.04287T + 5.31710 \times 10^{-5} T^2 + (0.00538 - 2.78208 \times 10^{-5} T + 3.74529 \times 10^{-8} T^2) \times 10^{-5} p \quad (\text{A.8})$$

Thermal conductivity:

$$k = \sum_{i=1}^3 \sum_{j=1}^3 \alpha_{ij} T^{j-1} p^{i-1} \quad (\text{A.9})$$

$$\mathbf{A} = \begin{pmatrix} 0.13924 & 3.78253 \times 10^{-5} & -2.89732 \times 10^{-7} \\ 6.27425 \times 10^{-11} & 6.08052 \times 10^{-13} & 3.64777 \times 10^{-16} \\ -1.38756 \times 10^{-19} & -2.57608 \times 10^{-22} & -2.70893 \times 10^{-24} \end{pmatrix} \quad (\text{A.10})$$

References

- [1] ExxonMobil. The outlook for energy: a view to 2040.
- [2] Jorach R, Judge R, Annycke B, Lamacchia F. Diesel common rail fuel systems technology for high efficiency ultra low emissions medium duty engines. In: IMechE conf fuel injection systems for IC engines, London.
- [3] Gavaises M. Flow in valve covered orifice nozzles with cylindrical and tapered holes and link to cavitation erosion and engine exhaust emissions. Int J Engine Res 2008;9(6):435–47.
- [4] Gavaises M, Papoulias D, Andriotis A, Giannadakis E, Theodorakakos A. Link between cavitation development and erosion damage in diesel injector nozzles. SAE technical paper 2007-01-0246.
- [5] Arcoumanis C, Badami M, Flora H, Gavaises M. Cavitation in real-size multi-hole diesel injector nozzles. SAE Trans J Engines, 2000-01-1249 109-3.
- [6] Prosperetti A, Hao Y. Modelling of spherical gas bubble oscillations and sonoluminescence. Philos Trans R Soc Lond Ser A 1999;357(1751):203–23.
- [7] Badock C, Wirth R, Fath A, Leipertz A. Investigation of cavitation in real size diesel injection nozzles. Int J Heat Fluid Flow 1999;20(5):538–44.
- [8] Chaves H, Knapp M, Kubitzek A, Obermeier F. Experimental study of cavitation in the nozzle hole of diesel injectors using transparent nozzles. SAE technical paper 950290.
- [9] Soteriou C, Andrews R, Smith M, Torres N, Sankhalpara S. The flow patterns and sprays of variable orifice nozzle geometries for diesel injection. SAE technical paper 2000-01-0943.
- [10] Blessing M, Knig G, Krger C, Michels U, Schwarz V. Analysis of flow and cavitation phenomena in diesel injection nozzles and its effect on spray and mixture formation. SAE technical paper 2003-01-1358.
- [11] Andriotis A, Gavaises M, Arcoumanis C. Vortex flow and cavitation in diesel injector nozzles. J Fluid Mech 2008;610:195–215.
- [12] Lai M-C, Zheng Y, Xie X-B, Moon S, Liu Z, Gao J, et al. Characterization of the near-field spray and internal flow of single-hole and multi-hole sac nozzles using phase contrast X-ray imaging and CFD. SAE Trans J Engines 2011;4(1):703–19.
- [13] Chen YL, Heister SD. Two-phase modeling of cavitated flows. Comput Fluids 1995;24(7):799–809.
- [14] Alajbegovic A, Grogger HA, Philipp H. Calculation of transient cavitation in nozzle using the two-fluid model. In: 12th ILASS-America; 1999.
- [15] Yuan W, Schnerr GH. Cavitation in injection nozzles – effect of injection pressure fluctuations. In: CAV2001, 4th int symposium on cavitation; 2001.
- [16] Schnerr GH, Sauer J. Physical and numerical modelling of unsteady cavitation dynamics. ICMF 2001, 4th int conf on multiphase flows.
- [17] Singhal AK, Athavale MM, Li HY, Jiang Y. Mathematical basis and validation of the full cavitation model. In: 2001 ASME fluid eng meeting; 2001.
- [18] Jamaluddin A, Ball G, Turangan C, Leighton T. The collapse of single bubbles and approximation of the far-field acoustic emissions for cavitation induced by shock wave lithotripsy. J Fluid Mech 2011;677:305–41.
- [19] Ando K, Colonius T, Brennen C. Numerical simulation of shock propagation in a polydisperse bubbly liquid. Int J Multiphase Flow 2011;37:596–608.
- [20] Fuster D, Colonius T. Modelling bubble clusters in compressible liquids. J Fluid Mech 2011;1:1–38.
- [21] Zeravic Z, Lohse D, Saarloos W. Collective oscillations in bubble clouds. J Fluid Mech 2011;680:114–49.
- [22] Joensen E, Colonius T. Numerical simulations of non-spherical bubble collapse. J Fluid Mech 2009;629:231–62.
- [23] Brennen CE. Cavitation and bubble dynamics. Oxford University Press; 1995.
- [24] Hilgenfeldt S, Brenner MP, Grossmann S, Lohse D. Analysis of Rayleigh–Plesset dynamics for sonoluminescing bubbles. J Fluid Mech 1998;365:171–204.
- [25] Keller J, Miksis M. Bubble oscillations of large amplitude. J Acoust Soc Am 1980;68(2):628–33.
- [26] Sakashita H, Ono A. Boiling behaviors and critical heat flux on a horizontal plate in saturated pool. Int J Heat Mass Transfer 2009;52:744–50.
- [27] Caira M, Cipollone E, Cumo M, Naviglio A. Forced convective boiling in high pressure parallel flow in tube bundles. Nucl Eng Des 1987;99:25–9.
- [28] Giannadakis E, Gavaises M, Arcoumanis C. Modelling of cavitation in diesel injector nozzles. J Fluid Mech 2008;616(1):153–93.
- [29] Giannadakis E, Gavaises M, Theodorakakos A. The influence of variable fuel properties in high-pressure diesel injectors. SAE technical paper 2009-01-0832.
- [30] Staedtke H. Gasdynamic aspects of two-phase flow. Wiley-VCH Verlag GmbH and Co. KGaA; 2007.
- [31] Bird RB, Stewart WE, Lightfoot EN. Transport phenomena. 2nd ed. John Wiley and Sons; 2007.
- [32] Kolev N. Multiphase flow dynamics 3: turbulence, gas absorption and release, diesel fuel properties. Berlin (Heidelberg): Springer Verlag; 2002.
- [33] Theodorakakos A, Mitroglou N, Gavaises M. Simulation of heating effects caused by extreme fuel pressurisation in cavitating flows through diesel fuel injectors. In: CAV2012; 2012.
- [34] Moukalled F, Darwish M. A unified formulation of the segregated class of algorithms for fluid flow at all speeds. Numer Heat Transfer Part B – Fundament 2000;37(1):103–39.
- [35] Moukalled F, Darwish M. Pressure-based algorithms for multifluid flow at all speeds – part I: mass conservation formulation. Numer Heat Transfer Part B – Fundament 2004;45(6):495–522.
- [36] Moukalled F, Darwish M. Pressure-based algorithms for multifluid flow at all speeds – part II: geometric conservation formulation. Numer Heat Transfer Part B – Fundament 2004;45(6):523–40.
- [37] Jasak H, Weller H, Gosman A. High resolution NVD differencing scheme for arbitrarily unstructured meshes. Int J Numer Methods Fluids 1999;31(2):431–49.
- [38] Giannadakis E, Papoulias D, Gavaises M, Arcoumanis C, Soteriou C, Tang W. Evaluation of the predictive capability of diesel nozzle cavitation models. SAE technical paper 2007-01-0245.